DEVELOPMENT OF AIRBORNE EDDY-CORRELATION FLUX MEASUREMENT CAPABILITIES FOR REACTIVE OXIDES OF NITROGEN

First Year's Progress Report on NAG-4699
and Request for Second Year Renewal

Prepared By:

Dr. John Bradshaw, Principal Investigator
Dr. Scott T. Sandholm, co-investigator
and Dr. Xiaonan Zheng, co-investigator
Georgia Institute of Technology
School of Earth and Atmospheric Sciences
Atlanta, Georgia 30332-0340
(Phone: (404) 894-3895)

TABLE OF CONTENTS

I. Overview of Objectives and Project Rationale

This research is aimed at producing a fundamental new research tool for characterizing the source strength of the most important compound controlling the hemispheric and global scale distribution of tropospheric ozone. Specifically, this effort seeks to demonstrate the proof-of-concept of a new general purpose laser-induced fluorescence based spectrometer for making airborne eddy-correlation flux measurements of nitric oxide (NO) and other reactive nitrogen compounds. The new all solid-state laser technology being used in this advanced sensor will produce a forerunner of the type of sensor technology that should eventually result in highly compact operational systems. The proof-of-concept sensor being developed will have over two orders-of-magnitude greater sensitivity than present-day instruments. In addition, this sensor will offer the possibility of eventual extension to airborne eddy-correlation flux measurements of nitrogen dioxide (NO_2) and possibly other compounds, such as ammonia (NH_3), peroxyradicals (HO_2), nitrateradicals (NO_3) and several iodine compounds (e.g., I and IO).

Demonstration of the new sensor's ability to measure NO fluxes will occur through a series of laboratory and field tests. This proof-of-concept demonstration will show that not only can airborne fluxes of important ultra-trace compounds be made at the few parts-per-trillion level, but that the high accuracy/precision measurements currently needed for predictive models can also. These measurement capabilities will greatly enhance our current ability to quantify the fluxes of reactive nitrogen into the troposphere and significantly impact upon the accuracy of predictive capabilities to model O_3's distribution within the remote troposphere. This development effort also offers a timely approach for producing the reactive nitrogen flux measurement capabilities that will be needed by future research programs such as NASA's planned 1999 Amazon Biogeochemistry and Atmospheric Chemistry Experimental portion of LBA.

II. Progress Report on First Year's Effort

As we proposed, the first two year's efforts were to concentrate on two primary areas: (1) the development of methodology for carrying out real-time continuous isotopic dilution calibrations; and (2) establishing the design criteria and initial design constraints for the flow line, sample cell, and other new system components. The isotopic dilution calibration work involves; (1) establishing the photodynamic basis of the technique including the effects of changes in pressure, temperature, and humidity (or absolute H_2O) on the sensitivity of both the ^{14}NO and ^{15}NO signal strengths; (2) establishing the factors limiting precision and accuracy; (3) developing an inert standard addition inlet system for use with a large diameter ram-air fed inlet; and (4) developing the rapid step function wavelength drive for the MOPO-730 laser. Also during the second year's effort, final designs for all major new system components are to be completed, including airworthiness and component stress analysis, along with fabrication of many of these systems. In addition, the new laser system hardware is to be repackaged into an aircraft flight worthy configuration. During the first year, significant progress has been made on all of these fronts.

Specifically, we are now capitalizing on the target of opportunity to deploy our new sensor package onboard NASA's DC-8 aircraft during the field 1996 NASA PEM-Tropics program. To accomplish this, we have accelerated this innovative research project's instrument development

efforts in order to provide a synergistic overlap with the primary non-developmental field mission objectives of our PEM-Tropics program support. This will enable us to use the PEM-Tropics airbone activity opportunity to provide an improved (e.g. demonstrating a large portion of the sensitivity improvements we have proposed) faster response NO sensor on PEM-Tropics while enabling us to test several of the even more advanced sensor concepts that will be needed for the flux instrument.

A. Development of the TP-LIF Based Spectrometer

Significant improvements in sensitivity will result from our incorporation of currently available laser and electro-optic technology (e.g., an approximate 100-fold improvement in the sensitivity for NO compared to the sensor deployed on NASA's 1994 PEM-WB program). The MP-LIF sensor to be deployed on PEM-Tropics during the Fall 1996 will enable a new analysis realm to be explored through its ability to make real-time high precision measurements at high enough frequencies to allow cross-correlation techniques to be applied to the analysis of co-variance with respect to other parameters (e.g., ±5% for NO @10 pptv and @1 Hz in conjunction with high speed measurements of H_2O, CO, O_3, temperatures, and UV intensity). This type of analysis can then be used to extract the information contained within the pervasive fine structure found in the remote troposphere (e.g., Newell et al., [1994]). This increased sensitivity will also enable the MP-LIF sensor to quantitatively measure other atmospherically important compounds (e.g., I, HO_2, and OH) at the parts per quadrillion levels anticipated in the remote atmosphere.

Table I gives the anticipated MP-LIF NO sensor's level of performance that is anticipated for NASA's summer 1996 PEM-Tropics airborne field program. The improvements in sensitivity result from four basic modifications that are currently being incorporated into the sensor package. The first improvement involves the straightforward 2-fold increase in sensitivity that results from increasing the number of dichroic filter/CsTe PMT assemblies from two to four, and a two-fold improvement resulting from refinements in a second generation of the new optical filter design. Most of the remaining improvements center around the incorporation of higher power laser and optical parametric oscillator technologies.

The optical schematic for the TP-LIF portion of the sensor is depicted in Figure 1. In this configuration an injection seeded Nd:YAG laser will be used as the primary pump laser source. This laser is capable of producing higher energy, narrower linewidth output at higher pulse rates than our previous laser system while using less space and electrical power. In the new sensor configuration, the Nd: YAG laser will be used to pump two narrow linewidth (< 0.2 cm^{-1}) master oscillator/power oscillator optical parametric oscillator systems MOPO-730. The frequency doubled output of one MOPO-730, will be used to generate mJ/pulse levels of narrow linewidth tunable 226 nm energy to excite the NO $X^2\Pi \rightarrow A^2\Sigma$ transition (<0.3 cm^{-1} compared to the current laser's ~1 cm^{-1}). The second infrared (IR) MOPO-730, will be used to generate >10 mJ per pulse of narrow linewidth (<0.2 cm^{-1}) tunable 1.1 μm energy to excite the $A^2\Sigma \rightarrow D^2\Sigma$ transition. An additional 5-fold increase in sensitivity will be obtained by using stronger lines in the $A^2\Sigma \rightarrow D^2\Sigma$ transition that have more optimal overlap between the ro-vibronic resolved NO absorption line and the laser linewidth (based on sensitivity improvement between an independently tunable and the "pseudo-fixed" wavelength of our previous system [Sandholm

et al., 1990]). A final 5-fold sensitivity increase will be obtained from the significantly larger available excitation energies at 226 nm, and 1.1 μm (i.e., ~5 mJ vs. ~1 mJ, and > 10 mJ vs. 0.7 mJ, respectively).

Even with the above improvements in sensitivity, the laser generated background will remain negligible. In the PEM-WB sensor, laser background noise was < 3 counts/180 seconds under all tropospheric sampling conditions. Since the sensitivity improvements discussed above will be used to obtain higher sub-second time resolution for a given level of NO, the new sensor will continue to be signal limited rather than background noise limited even at an NO level of 1 pptv or below. In addition, the narrow linewidth of the IR-MOPO systems will enable sufficient spectroscopic segregation of ^{15}NO from ^{14}NO to allow ^{15}NO to be used as an internal standard and in an isotopic dilution mode. In combination with the rapid tunability of all solid state laser system, this capability will increase precision and accuracy by enabling more rapid in-flight calibration approaches to be implemented using ^{15}NO for isotopic dilution at levels near those of ambient ^{14}NO. Thus, NO calibrations can be obtained even at the few pptv level and during conditions where ambient variability results in large changes in ^{14}NO with time.

B. Development of Quantitative Photofragmentation Detection PNO_2

Recently, concerns have arisen about possible interferences in the arc-lamp based photolytic conversion technique we have used to measure NO_2 [e.g., Crawford et al., 1994]. As with most photolytic convertors used to date, ours should have been free from the results of either gas phase thermal or photolytic decomposition of known potential interferants (e.g., HO_2NO_2, N_2O_5, or HNO_3). However, tests for these effects on previous systems have been inconclusive because the simple use of modest flow rate and temperature variations is not expected to be revealing if the interference is produced by wall-catalyzed rather than gas phase processes. For example, if the reaction probability at the wall is greater than approximately 10^{-4}, then large decomposition efficiencies and corresponding interferences can be expected over the entire range of possible operating conditions previously used [Sandholm et al., 1994]. This potential problem might also be expected to exhibit a substantial hystersis based on recent reports [Li et al., 1996] of HO_2 NO_2's surface absorption properties.

To eliminate this potential problem, the new sensor will use a high efficiency Nd:YAG laser photolysis source that will enable the MP-LIF sensor to use significantly more selective photolytic conversion schemes (i.e. similar to that developed for ambient NH_3). For NO_2, a single 8 ns laser pulse can be used to quickly carry out the photolysis step with high efficiency. Quantitatively carrying out the photolytic conversion in a single laser pulse will enable us to greatly minimize potential interferences from wall-catalyzed thermal and photolytic processes through the use of a sampling design system that capitalizes on the independence of the TP/LIF technique's signal strength and sensitivity on the flow rate through the sensor. The new sensor will use a large volume-to-surface ratio sampling manifold that is fed at high flow-rates (~3 x 10^4 lpm) using ram-air. This configuration will "turn-over" the sample faster than the laser pulse rate (i.e., sample residence time through instrument <0.05 s). The total residence time will be 100-fold shorter than in our previous sensors. The shorter residence time of this large diameter (10 cm) flow system will eliminate the possibility of interferences from wall-catalyzed decomposition of thermally labile nitrogen-containing compounds such as RO_2NO_2, even if the reaction

probability at the wall is unity. Wall-catalyzed photolytic interferences will also be eliminated as only the central portion of the flow field (<1 cm^2 of the 45 cm^2 full area) will be probed within 50 μs by the lasers.

The prototype sensor configuration to be deployed during the PEM-Tropic campaign will operate the primary TP-LIF portion of the laser system that generates the 226 nm and 1.1 μm NO fluorescence excitation laser beams at a pulse rate of 20 pps and the NO_2 photolysis laser will be "fired" on every other shot at 10 pps. A computer controlled (and adjustable) 50 μs delay will be used between the photolysis laser pulse and the TP-LIF NO fluorescence excitation laser pulses. This time delay will enable the nascent photofragmented NO population to repartition into an ambient temperature Boltzman distribution. In this scheme, a single fluorescence monitoring cell will be used to detect NO and NO_2 on alternate laser pulses. This configuration will increase the absolute accuracy of our NO_2 measurements by eliminating the subtle differences that can arise in previously used separate NO and NO_2 sampling cell arrangements. In addition, isotopic $^{15}NO_2$ can also be used in an internal standard and in an isotopic dilution mode (see earlier discussion on NO). Absolute accuracy of the NO and NO_2 ambient measurements using this approach are estimated at the 95% confidence limit to be ±8% and ±10% respectively.

The photolytic system can also be configured to produce a primary photolysis wavelength near 397 nm see Figure 2). The use of this longer photolysis wavelength will provide a significant means of testing for potential photolytic interferences from compounds such as HONO, alkyl-nitrates, and other odd-nitrogen-containing hydrocarbon compounds, which generally have large changes in absorption cross-sections between 355 nm and 397 nm (e.g., for HONO, $\sigma_{355\,nm} \sim 4 \times 10^{-19}$ cm^2 vs. $\sigma_{398\,nm} \sim 0.04 \times 10^{-19}$ cm^2). This longer photolysis laser wavelength will be generated via backward stimulated Raman frequency down conversion of the third harmonic (355 nm) of the Nd:YAG photolysis laser. This technique has been demonstrated in our laboratory to produce in excess of 70% photon conversion efficiencies [Bradshaw, 1989] and will generate a high quality laser beam with > 350 mJ of energy per pulse at 397 nm. The single laser pulse photolysis efficiency (E_p) for this scheme can be described by

$$E_p = [1-\exp(-P_p \sigma / a)]\phi \sim 0.7$$

where: P_p is the number of photons per laser pulse (P_p=7 x 10^{17} photons/pulse @ > 350 mJ), σ is the absorption cross section for NO_2 at 397 nm (σ=5.8 x 10^{-19} cm^2, Demore et al., 1992), a is the 397 nm laser beam cross sectional area (a=0.3 cm^2 for a 6 mm diameter beam), and ϕ is the quantum yield for production of NO at 397 nm (ϕ=0.87). The laser fluence used in this scheme is far below the onset of any non-linear behavior. In addition, the photolysis laser beam can be kept larger than the TP-LIF probe laser beams, thus minimizing problems with beam overlap and increasing measurement precision and accuracy. This basic photolysis scheme can be extended to compounds such as IO and NO_3.

C. Summary of Performance Goals

The improvements currently being incorporated into the next generation MP-LIF spectrometer will enable it to set a benchmark for making correct measurements under virtually any sampling condition. Several unique design features contribute to this sensor's robust performance, namely:

- *Spectroscopic specificity results from coincident excitation of separate ro-vibronically resolved electronic transitions and enables isotopic dilution/calibration techniques to be used;*

- *Freedom from background noise comes from the inherent nature of the multi-photon techniques used, making the sensor free from laser generated noise or changes in background even under high particle loading conditions (i.e., smoke, clouds, etc.);*

- *High confidence in measurements for transient (i.e., plume) events is assured by using multiple detectors and double coincidence signal processing techniques along with continuous monitoring of the instrument background, thus eliminating the possible effects from spurious noise sources (e.g., cosmic rays and EMI).*

- *MP-LIF spectrometer that is compatible with additions of future measurement capabilities (e.g. I and OH) using TP-LIF and PF-LIF (e.g. IO and NO_3) techniques and the use of new vibrationally mediated photofragment techniques (e.g. HO_2).*

D. Acquisition of New Laser System

The new Nd:YAG and MOPO laser systems have now been acquired and basically meet the specification goals we set for the sensitivity estimates provided in Table I. The new Nd:YAG laser is capable of generating sufficient 355 nm third harmonic energy to simultaneously pump two MOPO-730 optical parametric oscillators. This system produced >5mJ at 226 nm with a <0.25cm^{-1} linewidth and >10mJ in the 1.08 to 1.1 μm range with <0.15 cm^{-1} linewidth. In addition, as part of this project's effort, an aircraft worthy support structure has now been designed that structural analysis indicates will comply to the stringent (±100 μrad) beam alignment stability needed by the OPO system. Construction of this support system is now scheduled to begin using primarily second year funding resources from this program.

E. Development of Flowline and Sampling System

As part of our PEM-Tropics funded effort, a new external probe design is also now being fabricated for use on NASA's DC-8 aircraft. This probe will also be compatible with later use on the P-3B aircraft. In addition, we have designed it to allow us to use the high volume flow system we are actively developing as part of this innovative research project's flux sensor development effort. Specifically, as part of our first year effort on this project, we have also redesigned the entire flowline system to be fabricated using a newly available glass coated stainless steel technology. This will enable us to utilize ultra-high-vacuum component technology for the design of a clean/leak-free system that will combine the chemical inertness needed by an ambient sampling system. This flow manifold is currently being scheduled for fabrication as part of our second year effort. In addition, the system incorporates a

high velocity standard addition system which will be evaluated during the PEM-Tropics flights along with measurements from a more standard approach.

F. Development of Isotopically Labeled NO Technique as an Internal Standard in the TP/LIF NO Sensor

In order for the advanced airborne TP/LIF NO sensor to achieve high precision measurement ability in the convective boundary layer (CBL), a fast internal calibration system is needed to compensate the rapid change of environmental conditions. To accomplish this, we proposed a calibration method involving the use of isotopically labeled NO as an internal standard. In this scheme, a known amount of isotopically labeled NO (i.e., $^{15}N^{16}O$,$^{15}N^{18}O$, or $^{14}N^{18}O$) will be added into the sampling system continuously. The probe laser system will then be operated periodically between two modes, the "sample" mode and the "calibration" mode. In the sample mode, both probe laser wavelengths need to be optimized to specifically detect naturally abundant NO (*i.e.* $^{14}N^{16}O$) with minimal interference from the added isotopically labeled NO. Similarly, when the system is operated under the calibration mode, the laser wavelengths need to be optimized to specifically detect the isotopically labeled NO internal standard with negligible signal contributions from $^{14}N^{16}O$. With the rapid tunability of the probe lasers, the calibration frequency is only limited by the probe lasers' pulse repetition rate. For example, the calibration rate can be as high as 15Hz when the probe laser system tunes to the sample mode and the calibration mode alternatively with a 30Hz repetition rate laser. However, the success of the this calibration method is dictated by the spectral segregation between $^{14}N^{16}O$ and the isotopically labeled NO molecules for both excitation transitions (*i.e.* X→A and A→D) involved in the detection. In developing such a calibration system, we first need to spectroscopically study these transitions for both $^{14}N^{16}O$ and isotopically labeled NO under ambient atmospheric sampling conditions. As part of our first year research activity, we carried out an assessment based on both laboratory experiments and computer simulations.

A schematic of the experimental set-up that was used for the isotope studies is depicted in Figure 3. In this set-up, the second harmonic output (532 nm) of a Nd:YAG laser (DCR-3 Quanta-Ray) was used to pump a dye laser (PDL-2 Quanta-Ray) to generate visible light near 574 nm. The dye laser output was frequency doubled and then mixed in KD*P crystals with the residual fundamental Nd:YAG laser output (1.064 μm) to generated a tunable UV laser source near 226 nm. This UV laser was used to excite the NO ($X^2\Pi$, υ=0) → ($A^2\Sigma^+$, υ=0) transition. The second harmonic output of another Nd:YAG laser (DCR-1 Quanta-Ray) was also used to pump a dye laser (PDL-1 Quanta-Ray) in order to generate visible light near 574 nm. This dye laser output was directed through a high pressure (~ 150 psi) H_2 cell to generate a tunable IR laser source near 1.1 μm through the second stokes Raman shifting process. This IR laser was used to excite NO from the ($A^2\Sigma^+$, υ=0) state to the ($D^2\Sigma^+$, υ=0) state. The two laser beams were aligned to be collinear and passed through two flowing cells from opposite directions. Laboratory constructed pulse generators were used to trigger both Nd:YAG lasers. Time delay between the two trigger pulses was adjusted so that the UV (226 nm) laser beam reached the centers of the flow cells before the IR (1.1 μm) beam did. The fluorescence signal (i.e. $D^2\Sigma^+$ → $X^2\Pi$ emission) was detected using an optical filter

and photomultiplier tubes (PMT). The optical filters are highly selective against background light. Signals from both PMTs were fed into a laboratory constructed multichannel gated charge integrator (GCI) that acted as a peak sensing voltage to frequency convertor. Two computer controlled EG&G decade counters were then used to read and record the output from the GCI. Results from EG&G decade counters were stored in a personal computer.

During the experiments, 5ppmv of $^{14}N^{16}O$ in N_2 (from NIST) was sent into cell #1, while 10ppmv of either $^{15}N^{16}O$ or $^{15}N^{18}O$ in N_2 (from Scott-Marrin, Inc) was sent into cell #2. The spectra for both $^{14}N^{16}O$ and one of the isotopically labeled NO molecules were recorded simultaneously. The absolute laser frequency was calibrated by comparing recorded $^{14}N^{16}O$ spectral line positions with previous published results. The NO (X→A) transition has been studied extensively before and we have used the existing molecular constants to assess this transition. Because the NO (A→D) transition is much less understood, we focused our own experimental study on this latter transition system.

Figure 4-6 shows the experimental A→D spectra for $^{14}N^{16}O$ and $^{15}N^{18}O$ at different pressures. The spectra were recorded by fixing the broad bandwidth (~0.7cm^{-1}) UV laser wavelength on the overlapped P_{11} bandhead while scanning the IR laser. The time delay between the UV and IR lasers was about 15ns. Least squares fit of the peak positions in the $^{14}N^{16}O$ spectra to the published line positions yields the wavelength calibration of each spectra. Similar spectra were also recorded for $^{14}N^{16}O$ and $^{15}N^{16}O$. At the present laser linewidth, the spin-rotation splittings in both the A and D states were too small to be detected. Therefore, we used

$$E_r = B_\upsilon N(N+1)$$

to represent the rotational energy for both states, where B_0 is the rotational constant for the $\upsilon = 0$ state and N is the rotational quantum number. Rotational constants from a least squares fit of the recorded spectra based on equation (1) are given in Table 1. The second column in Table 1 gives the rotational constants calculated from isotope effect based on values for $^{14}N\ ^{16}O$ for both the A and D. Clearly, the measured and calculated values agree within the estimated uncertainties (+/- on standard error given in the parenthesis).

As can be seen from Figures 4-6, the A→D transitions show significant pressure broadening for both $^{14}N^{16}O$ and $^{15}N^{18}O$. The spectral line shape in Figure 4 can be treated as a convolution of the laser line shape with the line profile caused by pressure broadening. The spectra in Figure 6 were recorded at a pressure of 20 torr, thus the pressure broadening is negligible. At room temperature, the Doppler linewidth is about 0.02 cm^{-1} which is also negligible compared to the ~0.5cm^{-1} linewidth IR laser used in these experiments. Therefore, the spectral line shape in Figure 6 can be treated as the laser line shape. Deconvolution of the spectral lines in Figure 4 from those in Figure 6 yields the pressure broadening line profile. Here we have assumed the laser line shape follows a Gaussian function and the pressure broadening profile follows a Lorentzian function. The deconvolution results indicate that the pressure broadening linewidths for $^{14}N^{16}O$, $^{15}N^{16}O$ and $^{15}N^{18}O$ are all essentially the same with a value of 0.3±0.05 cm^{-1}atm^{-1}.

The actual lasers that will be used in the new airborne TP/LIF NO sensor will have much narrower linewidths in both the UV and IR regions. The actual UV linewidth will be about 0.2 cm^{-1}

and the IR laser linewidth will be about 0.15 cm^{-1}. Taking over pressure broadening measured value for the A→D transition and that for the X→A transition of $^{14}N^{16}O$ as about 0.6 $cm^{-1}atm^{-1}$. [Chang et al., 1993] and assuming $^{15}N^{16}O$ and $^{15}N^{18}O$ have the same pressure broadening linewidth for the X→A transition, we have simulated the X→A and A→D transitions using the narrower linewidth lasers under ambient atmospheric conditions. For these simulations, we have used the present and previous published molecular constants for the X, A, D states of $^{14}N^{16}O$ as well as the well known isotope effects in the electronic transitions (which have now also been verified). The simulated spectra are shown in Figure 7 and 8. These spectra were calculated for a Boltzmann distribution at a temperature of 298K.

In order to determine the optimal laser wavelengths for the sample mode and the calibration mode, we have to make a compromise between optimizing signal strength and minimizing unwanted overlap with the other isotope. Rotational energy transfer in the NO A state is very fast. However, if we simultaneously fire the UV and IR lasers, the rotational energy transfer will likely be only partially completed even at the ambient atmospheric pressure. Therefore, for this first iteration, we have selected transitions to obtain the maximum signal strength by tuning the IR laser to directly probe the rotational level prepared by the UV excitation. By examining the simulated spectra, several candidate pumping schemes appear very promising, for example the $R_1(9.5)$ & $Q_{21}(9.5)$ lines in the $^{14}N^{16}O$ X→A transition and the $P_1(10)$ & $P_2(10)$ lines in the $^{14}N^{16}O$ A→D transition in the sample mode. In the calibration mode, the UV and IR lasers will excite those same lines but for the $^{15}N^{16}O$ molecules. Figure 8 and 9 depict a blow-up of the simulated spectra near these spectral lines. These transitions originate from near the peak of the Boltzum rotational distribution and the absolute intensity for the $R_1(9.5)$ & $Q_{21}(9.5)$ lines are only about 25% smaller than the maximum intensity in the X→A transition. In addition, these rotational lines cleanly excite the NO molecule to a single rotational level in the A state, namely the $N = 10$ level. In this case, incomplete rotational energy transfer in the A state would be expected to result in the initial population in the A state remaining more concentrated in a single rotational level and therefore favor the signal strength of A→D transition. This may partially compensate the loss of signal strength due to the non-maximum excitation in the X→A step. When the lasers are tuned to these wavelengths, in the sample mode, the ratio between $^{14}N^{16}O$ and $^{15}N^{16}O$ signal strengths is estimated to be about 1140:1, whereas in the calibration mode the ratio between $^{14}N^{16}O$ and $^{15}N^{16}O$ signal strengths is about 1:2180. The above laboratory experiments and computer simulations indicate that $^{15}N^{16}O$ is a good candidate for use as an internal standard in our proposed advanced airborne TP/LIF NO sensor. The spectral segregation is sufficient enough that it is not likely to be the limiting factor when using commonly available isotopic purity standards (e.g. 99 atom percent), even at atmospheric pressure. These estimated ratios clearly indicate that we can use $^{15}N^{16}O$ as an internal standard without the need of reduced pressure operation, to reduce collision broadening as long as the concentration of the added $^{15}N^{16}O$ is close to that of the ambient $^{14}N^{16}O$ (within a factor of 10 to 100).

Further laboratory studies are needed. First, we need to better understand the rotational energy transfer in the A state. This information is needed in order to better characterize this state's rotational distribution that is being probed by the IR laser. This information will facilitate choosing

the IR laser wavelength to get the maximum performance out of the airborne TP/LIF NO sensor. Second, quenching of the A and D states also needs to be better understood in order to determine any limitations using of $^{15}N^{16}O$ as a calibration standard under the rapidly changing environmental conditions that will be encountered in a flux mode of operation. Third, we need to take experimental spectra of both the X→A and A→D transitions using the actual laser systems for to be used in the airborne sensor. These spectra will give us the actual experimental line shapes which are critical for the estimation of $^{14}N^{16}O$ and $^{15}N^{16}O$ signal strength ratios. These spectra will provide us final guidance for choosing the optimal wavelengths for the probe laser system. As part of the second year's effort, these experimental studies will be performed for both naturally abundant NO and isotopically labeled NO under various atmospheric conditions.

III. Second Year Proposal Research Plan

The second year's effort will be primarily focused on completing the first version of a prototype flux sensor that will be field tested during NASA's PEM-Tropics program. Sensor design and fabrication activities will continue at an accelerated pace with fabrication being completed for the Fall deployment. This effort will provide demonstration of much of the sensitivity improvement factors needed for the flux measurement sensor. Work will also continue on developing the spectroscopic and photodynamic basis for a real-time isotopic dilution technique in addition to designing the rapid wavelength tuning system for the MOPOs.

TABLE I. Anticipated Performance of NO and NO_2 Sensor To Be Deployed In PEM-Tropics

Frequency of Observation (signal integration time)	NO 5 Hz (0.2 sec)	NO 1Hz (1 sec)	NO 0.1 Hz (10 sec)	NO_2 1 Hz (1 sec)	NO_2 0.1 Hz (10 sec)
1. Horizontal Spatial Resolution @ 200 m/s air speed)	40 m	200 m	2 km	200 m	2 km
2. Vertical Spatial Resolution @ 300/m/min ascent/descent rate)	1 m	5 m	50 m	5 m	50 m
3. Measurement Precision (±1σ)					
@ 10 ppt NO	14%	6%	2%	4%	2%
@ 50 ppt NO	6%	3%	1%	8%	3%
Both @ 50 pptv NO_2					
4. Limit-of-Detection (S/N = 2/1)	1 pptv	0.2 pptv	<0.02 pptv	1 pptv (@55pptv NO)	1 pptv (@50pptv NO)
5. Total Sample Residence Time	<0.03 s	<0.03 s	<0.03 s	<0.03 s	<0.03 s
6. Base Data Recording Rate	20 Hz	20 Hz	20 Hz	10 Hz	10 Hz

Table 2. Rotational Constants for $A^2\Sigma^+$ ($\upsilon = 0$) and $D^2\Sigma^+$ ($\upsilon = 0$)

States of $^{14}N\ ^{16}O$, $^{15}N\ ^{16}O$, and $^{15}N\ ^{18}O$

	$A^2\Sigma^+$ (υ=0)		$D^2\Sigma^+$ (υ=0)	
	Measured	Predicted from isotope effect	Measured	Predicted from isotope effect
$^{14}N\ ^{16}O$	1.9830 (12)	----	1.9869 (12)	----
$^{15}N\ ^{16}O$	1.9137 (16)	1.9124	1.9167 (16)	1.9162
$^{15}N\ ^{18}O$	1.8092 (13)	1.8097(13)	1.8115 (13)	1.8132

Natural Abundance of Isotopes

$^{14}N\ ^{16}O = 99.39\%$
$^{15}N\ ^{16}O = 0.369\%$
$^{14}N\ ^{18}O = 0.203\%$
$^{15}N\ ^{18}O = 0.0008\%$

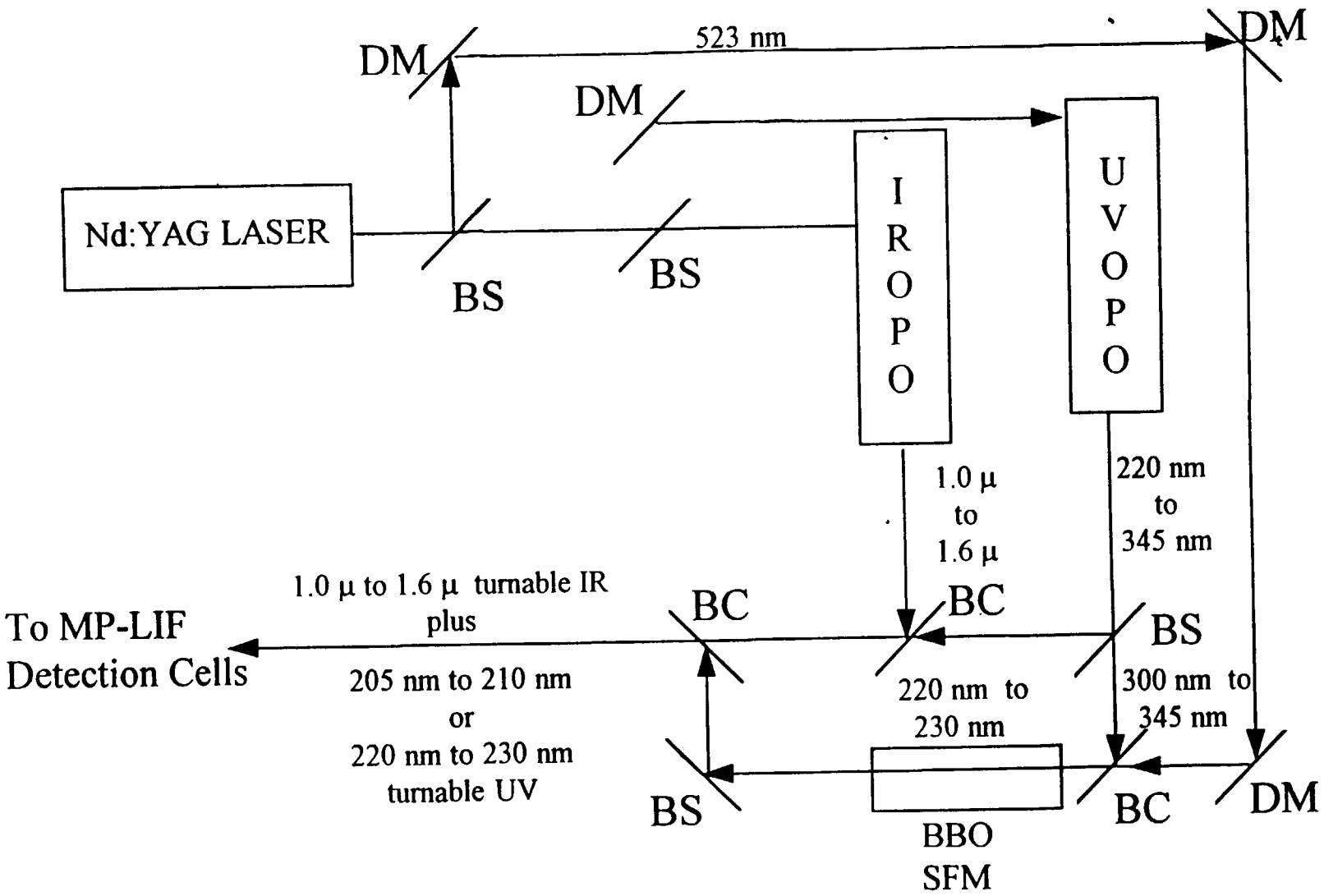
DM
523 nm
DM
DM
Nd:YAG LASER
BS
BS
I R O P O
U V O P O
1.0 μ to 1.6 μ
220 nm to 345 nm
1.0 μ to 1.6 μ turnable IR plus
205 nm to 210 nm or 220 nm to 230 nm turnable UV
To MP-LIF Detection Cells
BC
BC
BS
220 nm to 230 nm
300 nm to 345 nm
BS
BC
DM
BBO SFM

Figure 2.

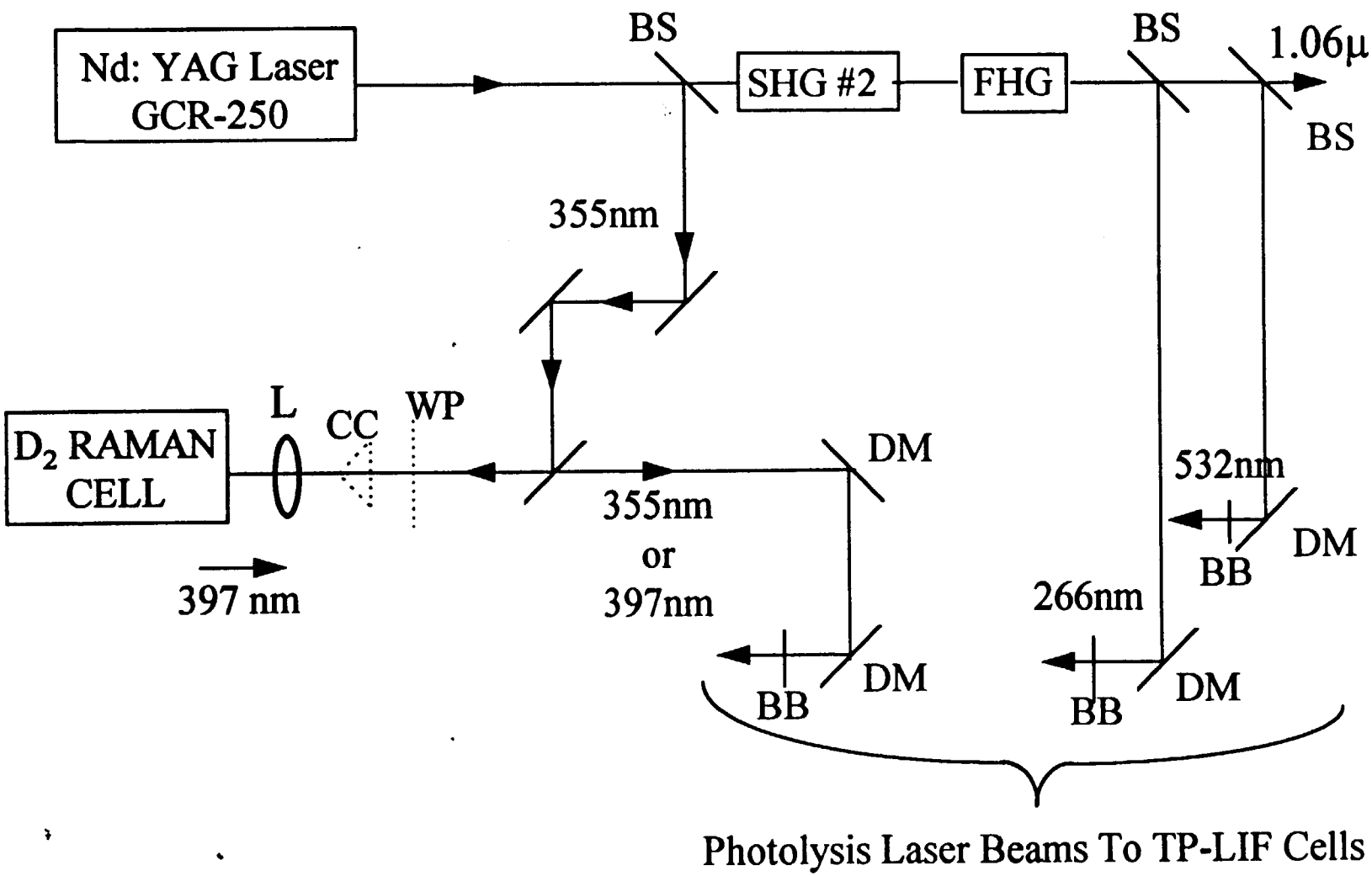
Nd: YAG Laser
GCR-250
BS
SHG #2
FHG
BS
1.06μ
BS
355nm
L
CC
WP
D2 RAMAN
CELL
DM
355nm
or
397nm
532nm
DM
BB
397 nm
266nm
BB
DM
BB
DM
Photolysis Laser Beams To TP-LIF Cells

Figure 3.

Figure 3

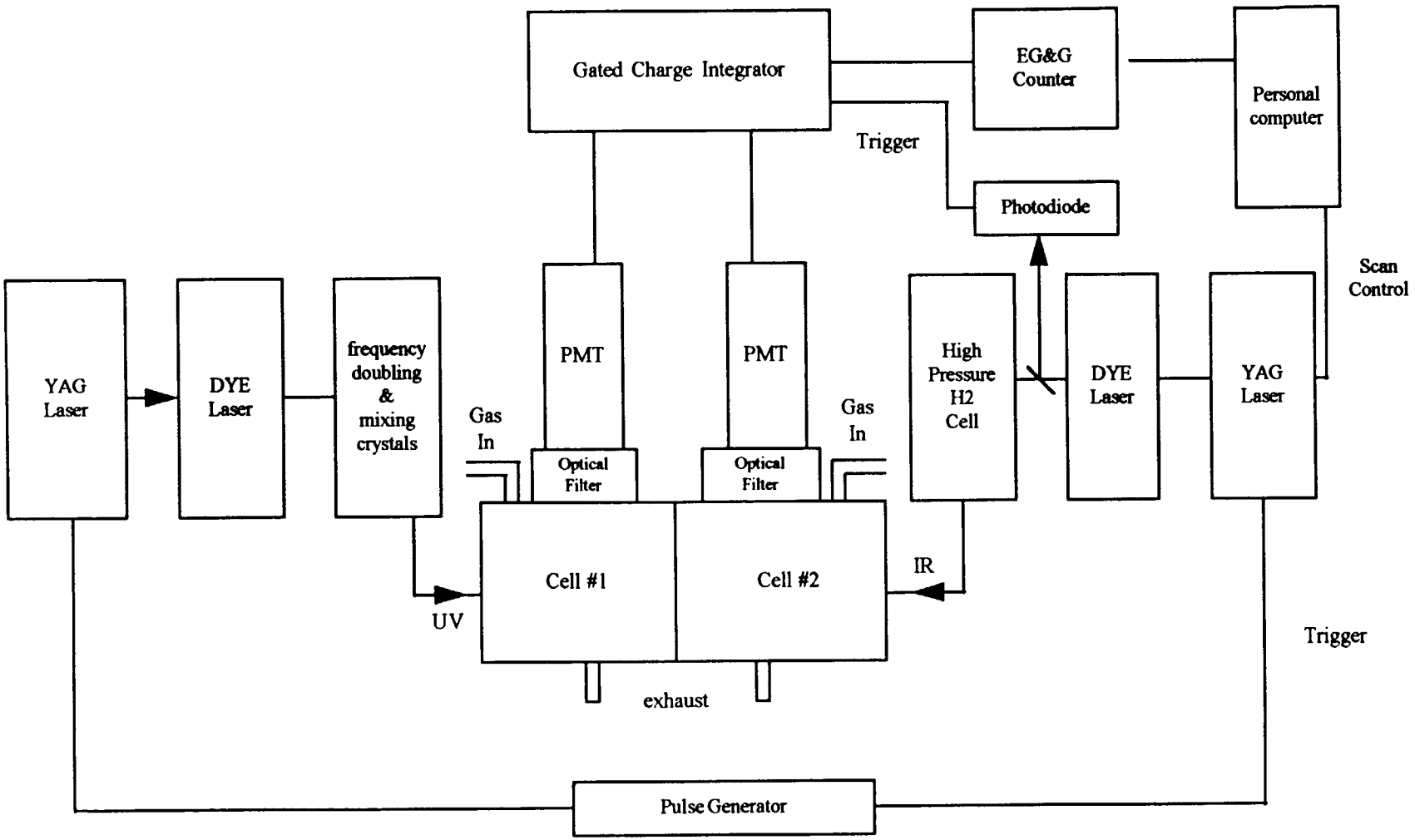
Gated Charge Integrator
EG&G Counter
Personal computer
Trigger
Photodiode
Scan Control
YAG Laser
DYE Laser
frequency doubling & mixing crystals
PMT
PMT
High Pressure H2 Cell
DYE Laser
YAG Laser
Gas In
Gas In
Optical Filter
Optical Filter
Cell #1
Cell #2
IR
UV
exhaust
Trigger
Pulse Generator

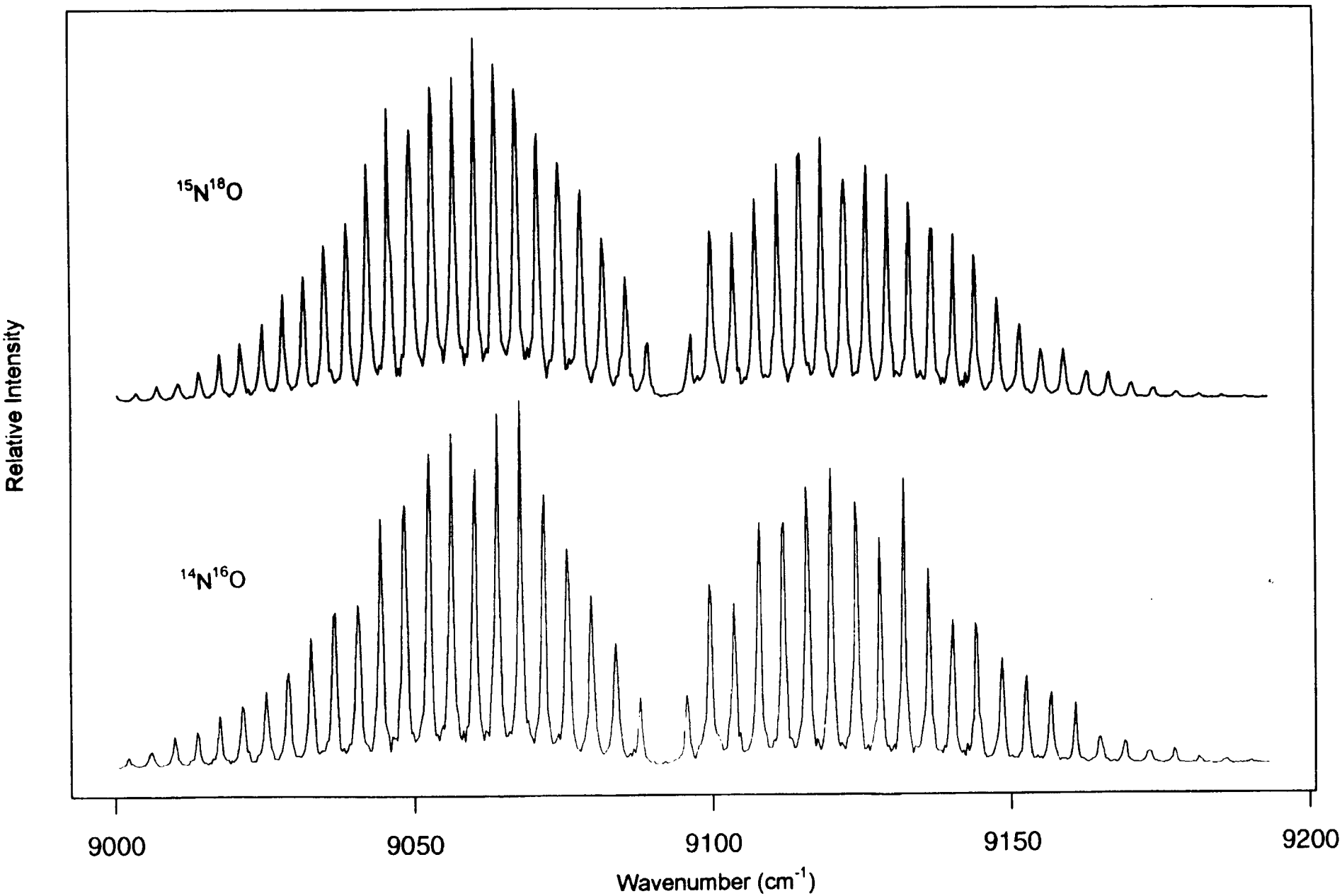

Figure 4. Fluorescence excitation spectra for the A→D transition for $^{14}N^{16}O$ versus $^{15}N^{18}O$ at 1atm pressure

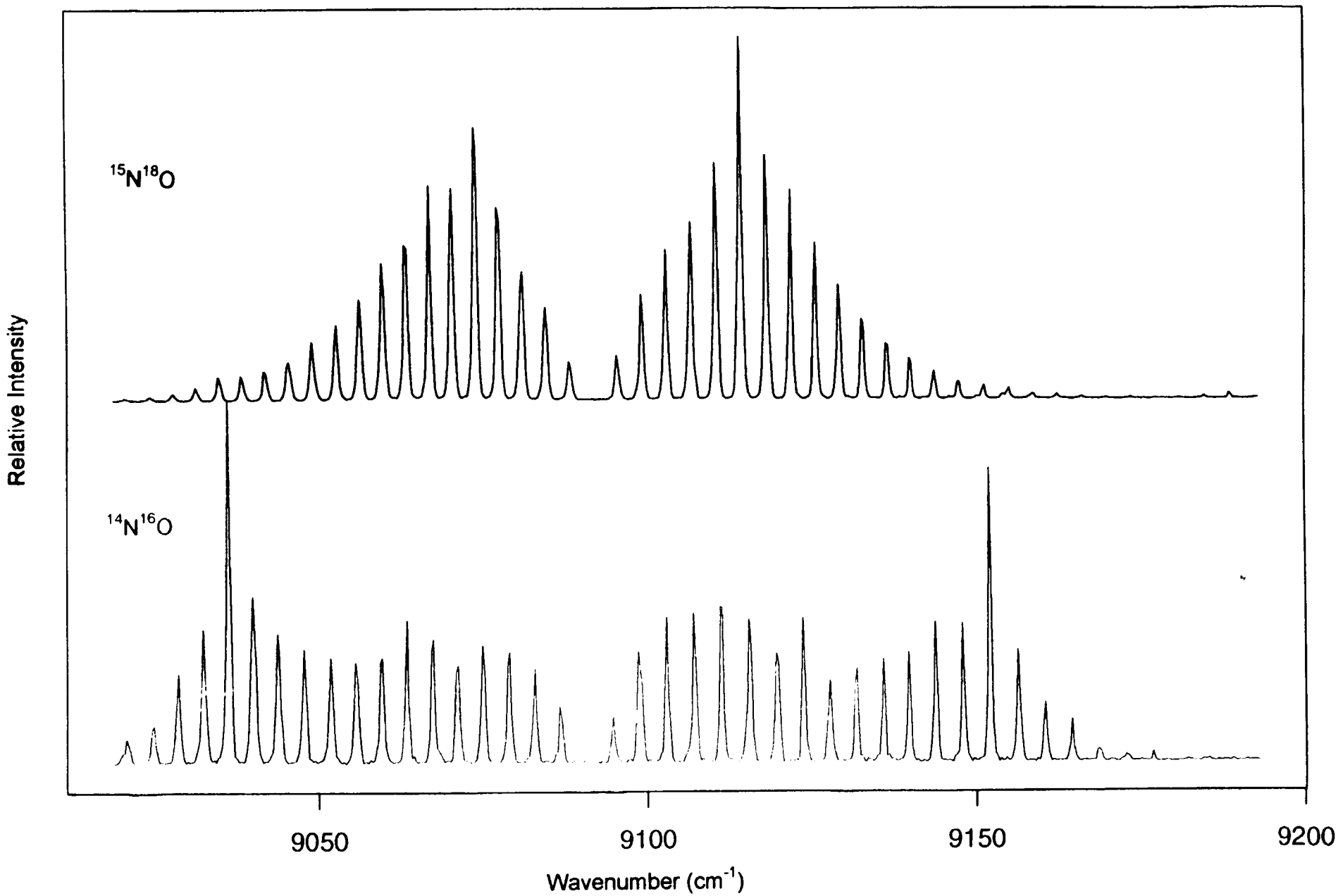

Figure 5. As Figure 4 except at 202 torr pressure

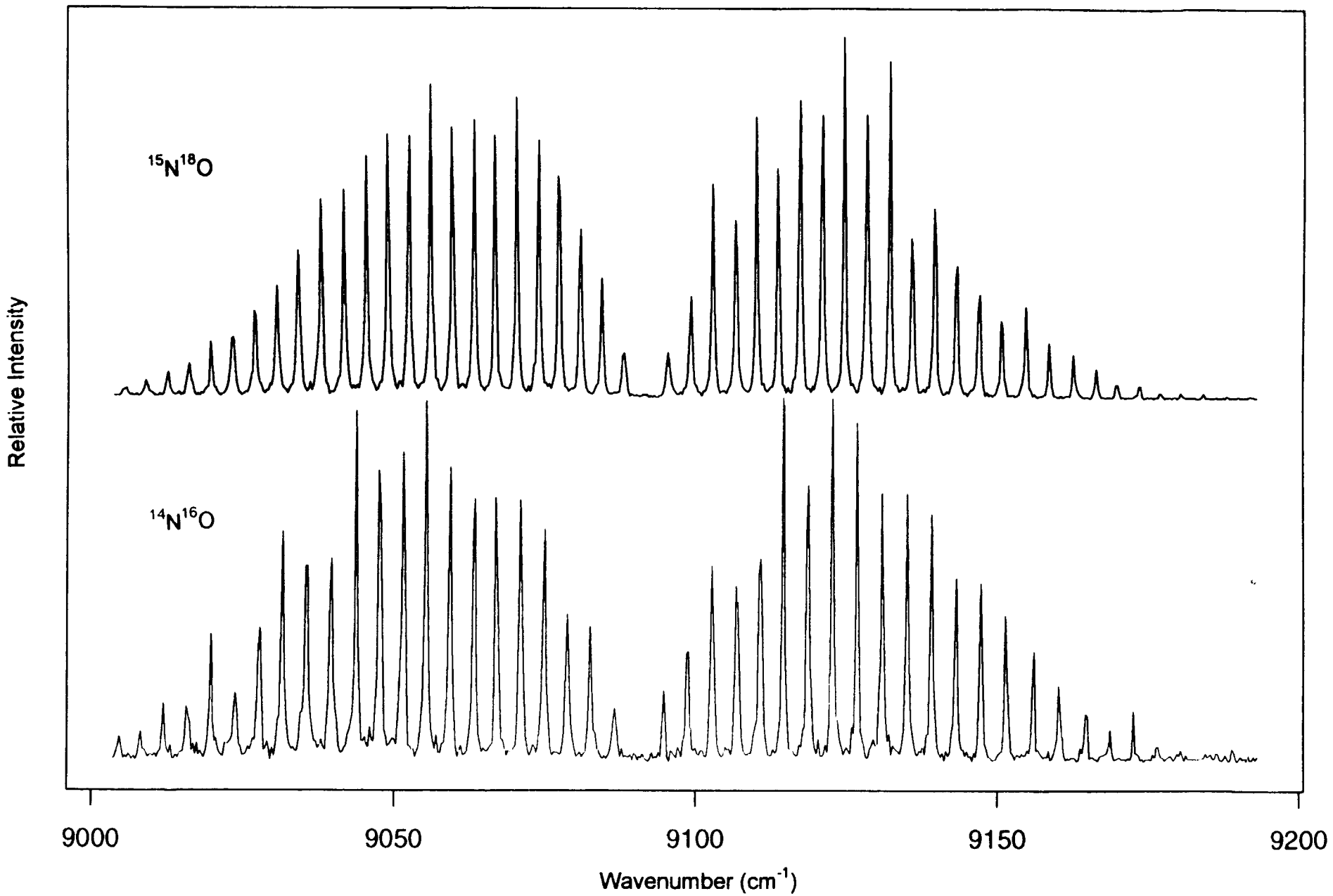

Figure 6. As Figure 4 except at 20 torr pressure

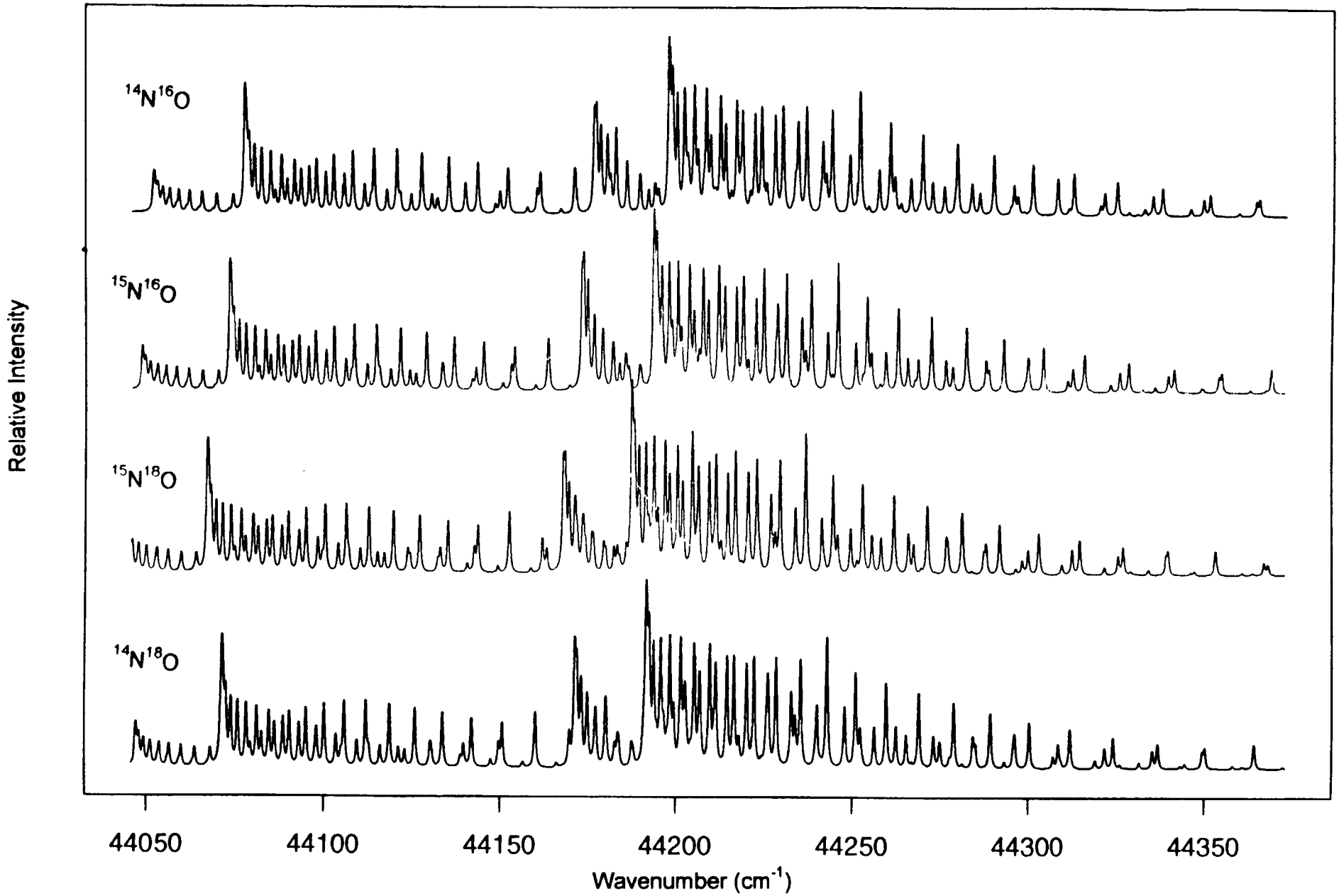

Figure 7. Simulated absorption spectra for the X→A transition for isotopes of NO at 1atm pressure and a 0.25 cm^{-1} laser linewidth

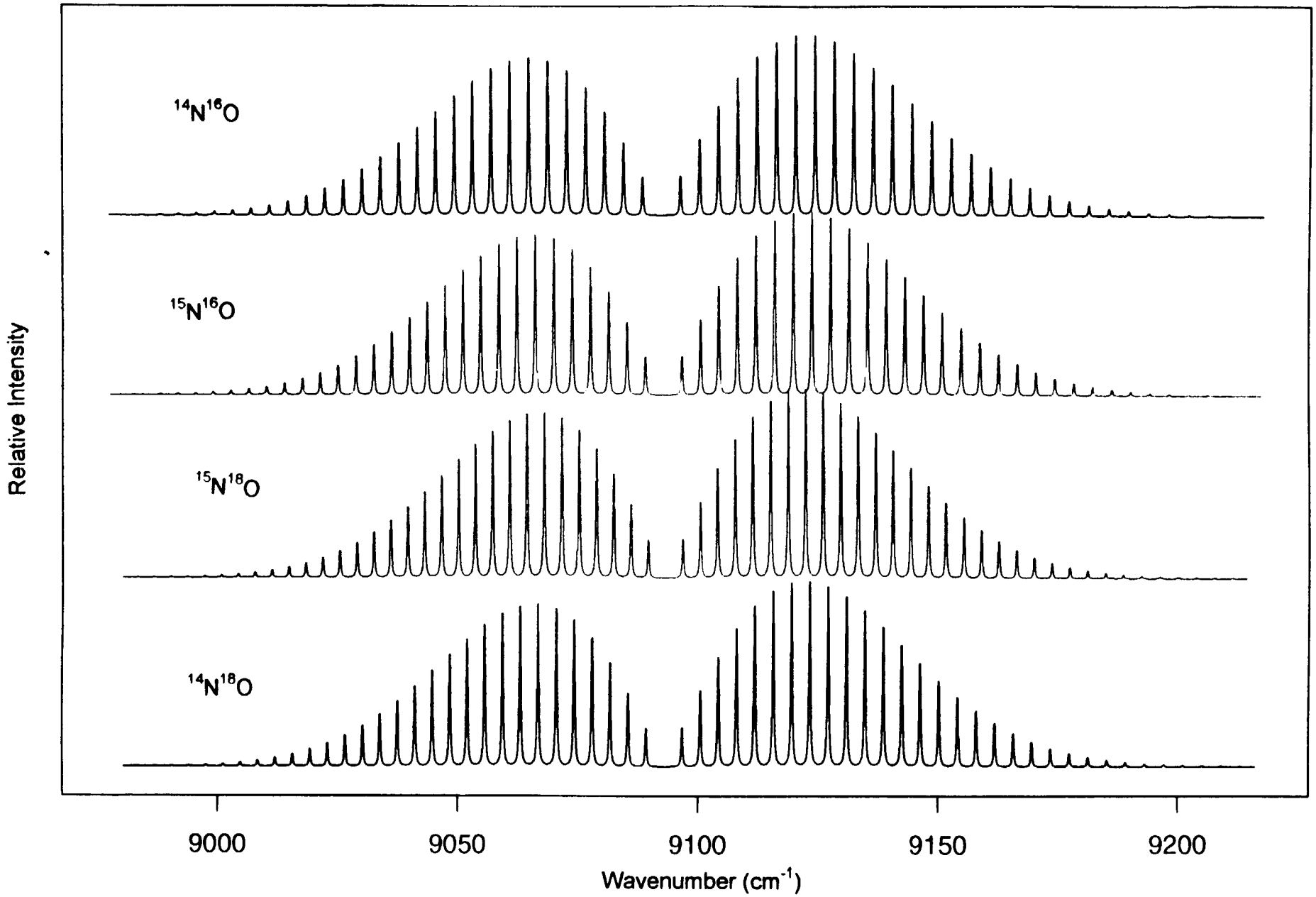

Figure 8. Simulated absorption spectra for the A→D transition for isotopes of NO at 1atm pressure and a 0.15 cm^{-1} laser linewidth

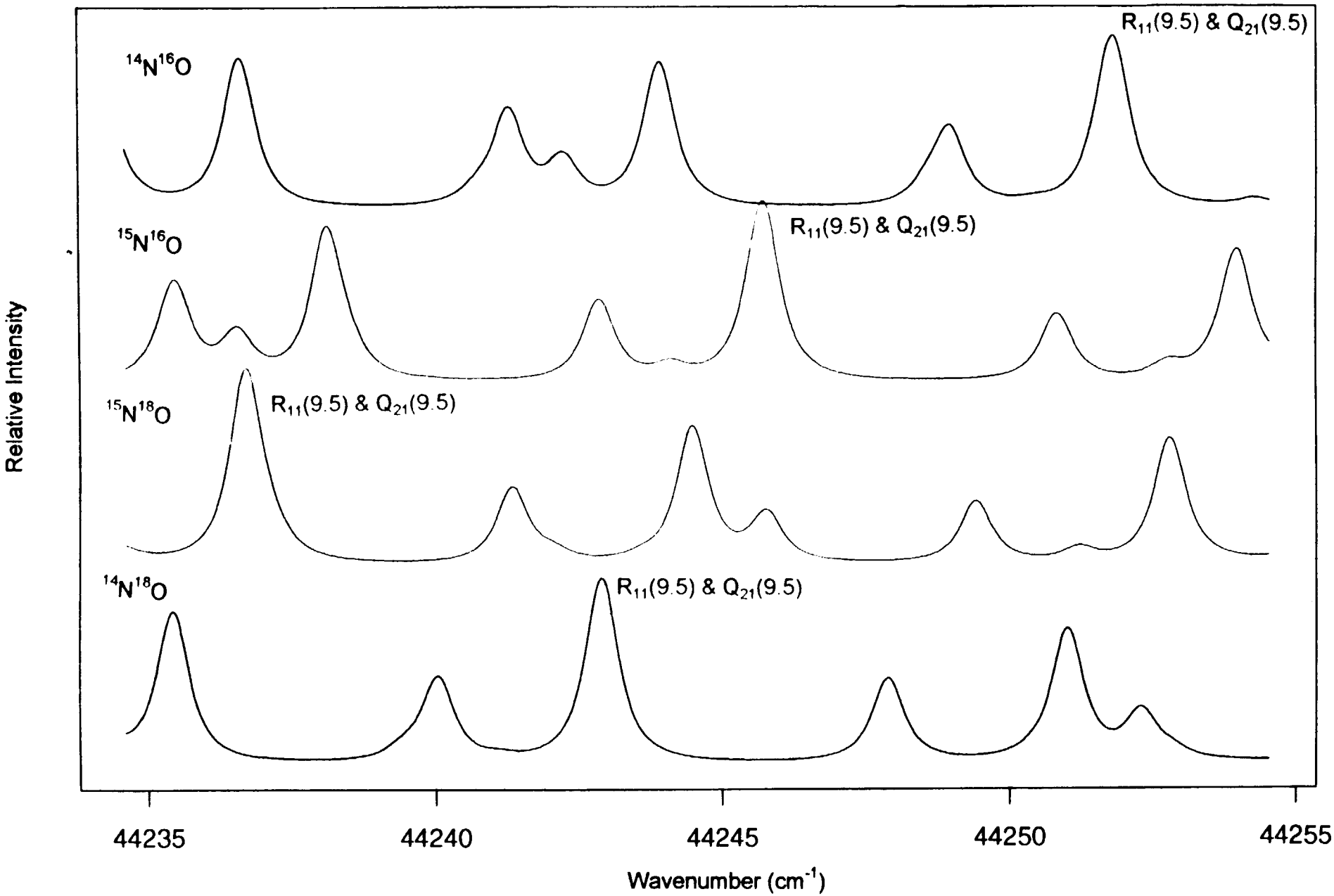

Figure 9. As Figure 7 except with expanded scale

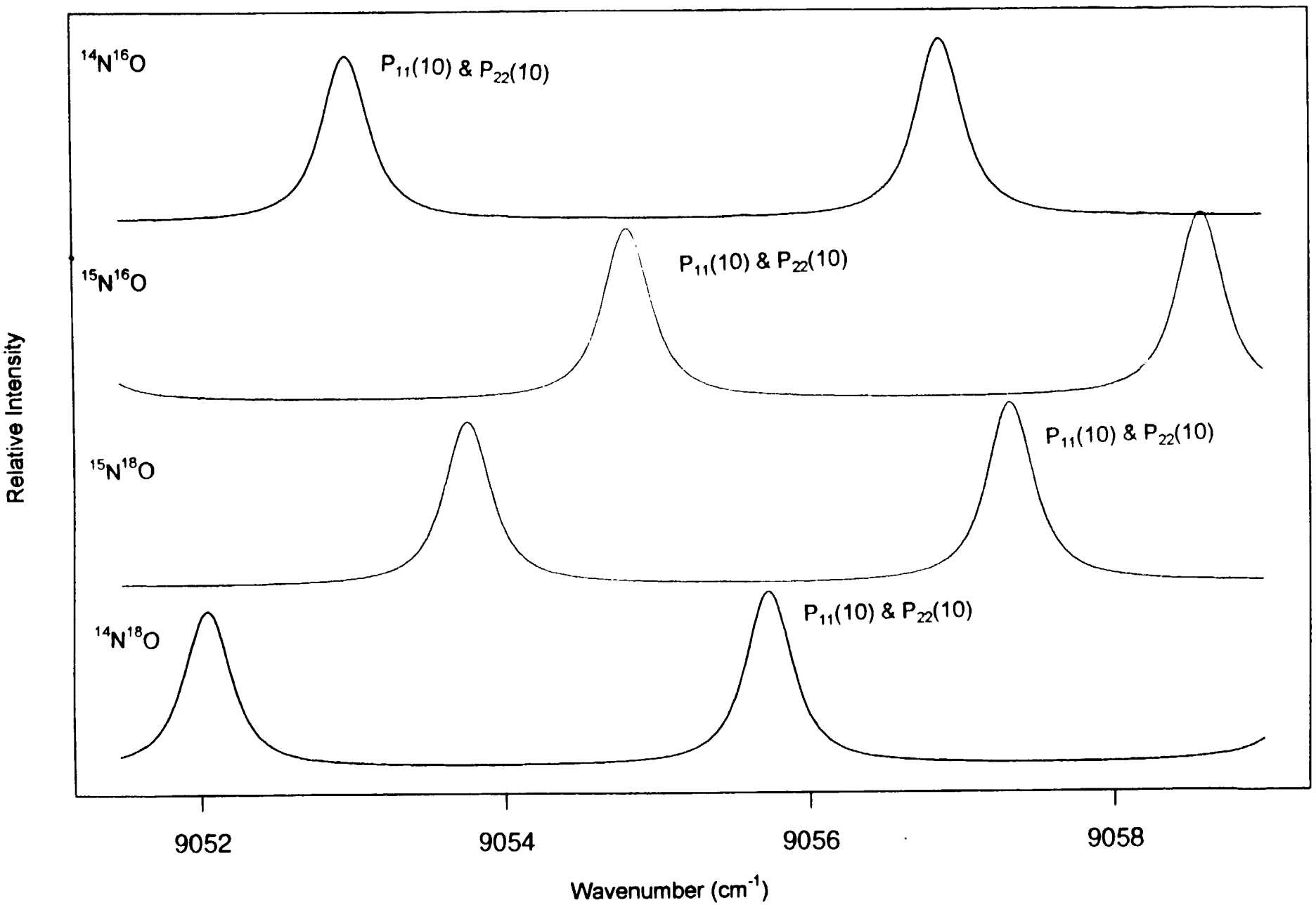

Figure 10. As Figure 8 except with expanded scale